Progress In Electromagnetics Research M, Vol. 40, 57–67, 2014

Intra-Body Propagation Channel Investigation Using Electrically Coupled Loop Antenna

Ali Ibraheem and Majid Manteghi*

Abstract—Knowledge of propagation media, typically gathered through physical experiments and simulations, is absolutely critical in successful transceiver design. In the case of medical implants, physical experiments are extremely difficult. Therefore, we rely on simulations in most studies. In this paper, Path Loss (PL) between implanted antennas, as a measure of propagation channel characteristics, is investigated using High Frequency Structure Simulator (HFSS) and Remcom's XFDTD 7 (XF7). An Electrically Coupled Loop Antenna (ECLA) is designed to study PL inside human body models at different frequency bands: Medical Implanted Communication Services (MICS) band (402–405 MHz), Industrial Scientific and Medical (ISM) band (2.4–2.5 GHz) and 3.5 GHz band (3.55–3.65 GHz). The ECLA has dimensions ($5 \times 5 \times 3\,\text{mm}^3$), ($3 \times 3 \times 3\,\text{mm}^3$) and ($2 \times 2 \times 2\,\text{mm}^3$) at MICS, ISM and 3.5 GHz respectively. ECLA performance inside human body models is studied at the allowed frequency bands. The effects of frequency bands, human model electrical properties, and distance between implants on PL are considered. Simulation results are validated with experimental work. Our results show that the ECLA at MICS band has the lowest Specific Absorption Rate (SAR) and the highest allowed input power. Also, the MICS band has the lowest PL inside the human body model, shown to be less than 90 dB in the worst case scenario.

1. INTRODUCTION

Nowadays, patients' health information can be collected and monitored remotely using biotelemetry wireless networks such as Wireless Body Area Network (WBAN). Implanted devices are the key components of WBAN [1], a promising technology in biotelemetry, e-health care, and hyperthermia applications. In the development of efficient WBAN applications, understanding the propagation channel characteristics is essential.

According to the Federal Communication Commissions (FCC) and European Radio-communication Commissions (ERC), the common frequency bands approved for implanted antennas can be classified into two categories: Narrowband (NB) and wideband. NB includes the Medical Implanted Communication Service (MICS) band, a growing standard, and Industrial Scientific and Medical (ISM) band. The MICS band has relatively low power loss inside the human body and is able to transmit its low data rate over a long range relative to previous technologies, though it needs a large antenna. On the other hand, the high-frequency systems are able to transmit at high data rates with a small antenna, but they have high propagation loss inside the human body [1].

The inductive coupling technique widely adopted in the primitive design of implantable devices is no longer appropriate for current biomedical systems. This is due to its low data rate and short communication range [2]. Recently, a considerable effort has been devoted to investigating the propagation channel inside the human body [2–11]. In previous works, the propagation channel at all allowed frequency bands was not investigated. The near-field characteristics of the implanted antenna,

Received 21 October 2014, Accepted 29 November 2014, Scheduled 9 December 2014

* Corresponding author: Majid Manteghi (manteghi@vt.edu).

The authors are with the Bradley Department of Electrical and Computer Engineering, Virginia Polytechnic Institute and State University, VA 24061, USA.

which plays an important role in the propagation channel, has been studied in [12]. In this work, intra-body propagation channel will be investigated for human body models using an Electrically Coupled Loop Antenna (ECLA) at the allowed frequency bands.

The paper will be organized as follows: In Section 2 ECLA structure will be described. ECLA performance inside different human body models at the allowed frequency bands will be investigated in Section 3. PL inside one-layer and three-layer models at the allowed frequency bands will be investigated in Section 4. Effects of the human body model on PL at MICS frequency band will be studied in Section 5. In Section 6, PL inside a simple model of the human body will be explored. Then, PL inside an exact human body model will be explained in Section 7. Experimental work and conclusions will be presented in Sections 8 and 9.

2. ECLA STRUCTURE

The ECLA is a magnetic field antenna introduced in [13] as a dual for electric field antennas, such as the Planar Inverted-F Antenna (PIFA) and patch antenna. This is because it has a relatively small near-zone electric field intensity, and as a result, small Specific Absorption Rate (SAR) inside the human body [14]. The ECLA consists of a high-impedance transmission line (distributed inductance) terminated to a short circuit at one end, and a distributed capacitance at the other end, forming an LC resonator. The distributed capacitance and feeding head are electrically coupled to the antenna as shown in Figure 1. The resonant frequency of the antenna is controlled by the antenna dimensions (L, W, and h) and the distributed capacitance between the loop and ground plane (t_s, W_s, and L_s). The input impedance of the antenna can be scaled to match a wide range of impedances by varying the feeding head dimensions (L_p, W_p, and t_p). Also, an ECLA can be used as a tunable antenna by adding a variable lumped capacitor in parallel with the distributed capacitor.

3. ECLA PERFORMANCE AT THE ALLOWED FREQUENCY BANDS

Simple models for the human body as one-layer and three-layer models, shown in Figure 2, are used to reduce the simulation time and problem complexity. After optimizing the antenna for each frequency

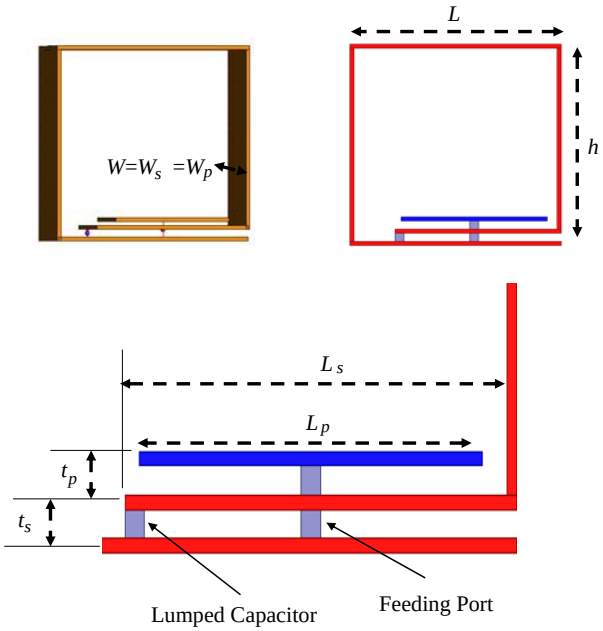

Figure 1. ECLA structure: front view and magnified view of feeding head and distributed capacitance part.

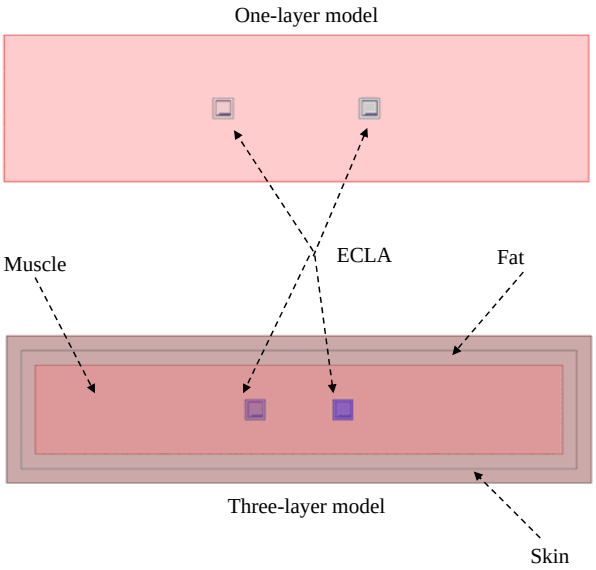

Figure 2. Two ECLAs inside one-layer and three-layer human body model.

range and computing primitive values for PL at different frequency ranges, the antenna will be simulated in a full human body model to compute the values for PL more accurately.

The performance of the ECLA inside one-layer and three-layer models are studied using High Frequency Structure Simulator (HFSS) at the allowed frequency bands. The ECLAs dimensions (L, h, W) have a value of $5\times5\times3\,\text{mm}^3$ (ECLA 1), $3\times3\times3\,\text{mm}^3$ (ECLA 2) and $2\times2\times2\,\text{mm}^3$ (ECLA 3) at MICS, ISM and 3.5 GHz frequency bands, respectively. Also, the ECLA is surrounded by a biocompatible insulation layer of 1 mm thickness with a relative dielectric constant of 2.07 and low loss. As the first example, a one-layer model with dimensions of $200\times50\times50\,\text{mm}^3$, which can simulate a human arm, has been used where the ECLA is located at the center of the model. This model has electrical properties of muscle and skin tissue at the allowed frequency bands shown in Table 1 [15]. The three-layer model consists of muscle with thickness of 35 mm, fat with thickness of 5 mm and skin with thickness of 2.5 mm. This model is shown in Figure 2.

The computed scattering parameters (S_{11}) of ECLAs at the allowed frequency bands are shown in Figure 3. The radiation characteristics (-3 dB bandwidth, 1 g averaged SAR for 1 W input power and maximum allowed input power) of ECLAs inside the human body models are shown in Table 2. Based on these results, as the frequency increases, ECLA dimensions decrease, -3 dB bandwidth increases and the value of SAR increases. Also, the ECLA is less sensitive to the detuning effect due to the electrical properties of human body tissues. According to the FCC and ERC, the maximum limits for SAR averaged over 1 g and 10 g of tissue mass are 1.6 W/kg and 2 W/kg, respectively [16, 17]. Due to the SAR limitation, the maximum allowed input power to the antenna decreases as the frequency increases.

Table 1. Dielectric properties of human body tissues at MICS, ISM and 3.5 GHz frequency bands.

Band	Tissue	Dielectric constant	Conductivity (S/m)	Density (kg/m^3)
MICS	Skin	49.85	0.67	1100
	Muscle	57.95	0.81	1040
	Fat	11.62	0.081	1850
ISM	Skin	42.85	1.59	1100
	Muscle	53.6	1.81	1040
	Fat	10.82	0.27	1850
3.5 GHz	Skin	41.41	2.35	1100
	Muscle	52.12	2.72	1040
	Fat	10.5	0.42	1850

Table 2. Radiation characteristics of ECLA inside human body models at MICS, ISM and 3.5 GHz frequency bands.

Band	Model	Bandwidth (MHz)	SAR 1 g (W/kg)	Max. P_{in} (mW)
MICS	Skin	5.53	144.2	11.1
	Muscle	5.83	148.3	10.8
	3-layers	5.73	193.8	8.3
ISM	Skin	330	264	6.1
	Muscle	363	266	6
	3-layers	330	269.1	5.95
3.5 GHz	Skin	380	383.5	4.2
	Muscle	413	405.2	3.95
	3-layers	369	409.6	3.91

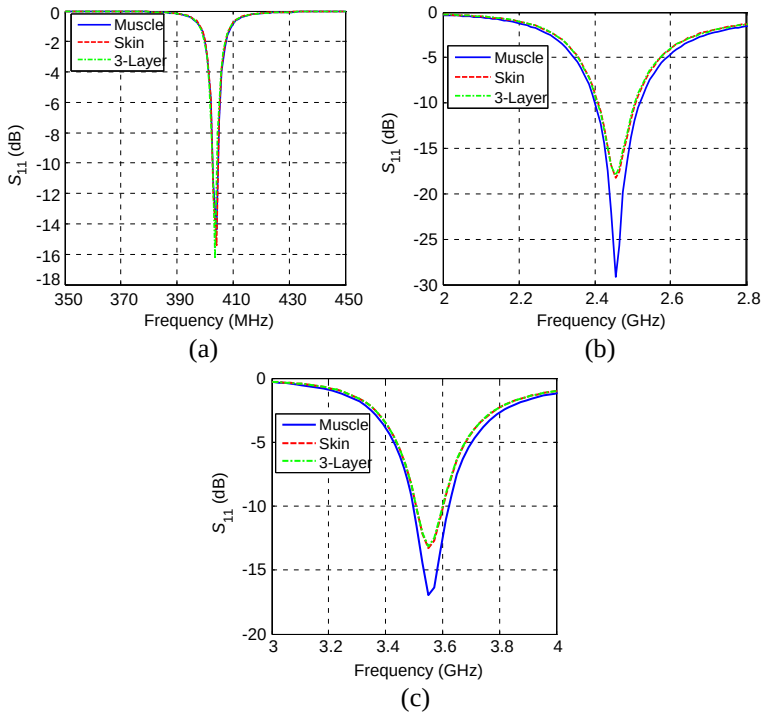

Figure 3. Scattering parameters (S_{11}) of ECLA inside human body models at (a) MICS band, (b) ISM band, and (c) 3.5 GHz band.

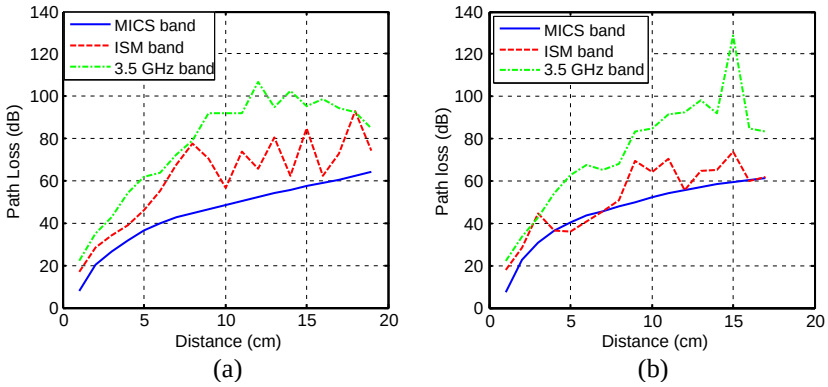

Figure 4. PL inside human body models (a) one-layer model and (b) three-layer model.

4. EFFECT OF FREQUENCY BAND ON PL

Electrical properties of human body tissues are functions of frequency, time, emotional mode, and diet. This fact makes the propagation phenomenon even more sophisticated for implanted antennas. The effect of increasing distance at three different frequency bands in one-layer and three-layer models is studied using HFSS and the results are shown in Figure 4. It is worth mentioning that these computed path losses include the antenna loss and mismatch loss as well. The magnitude of electric field intensity and real part of the Poynting vector inside a one-layer model at the allowed frequency bands at distance 100 mm between ECLAs are shown in Figures 5 and 6, respectively.

For a point source in a homogeneous lossy medium there is an exponential decay in addition to the spherical expansion factor, $1/r$. Although the human body is not a homogeneous medium, the short distance line-of-sight (LOS) path experiences an exponential decay which can be seen in Figure 4. Although the loss mechanism for small antennas is more sophisticated than a point source due to the

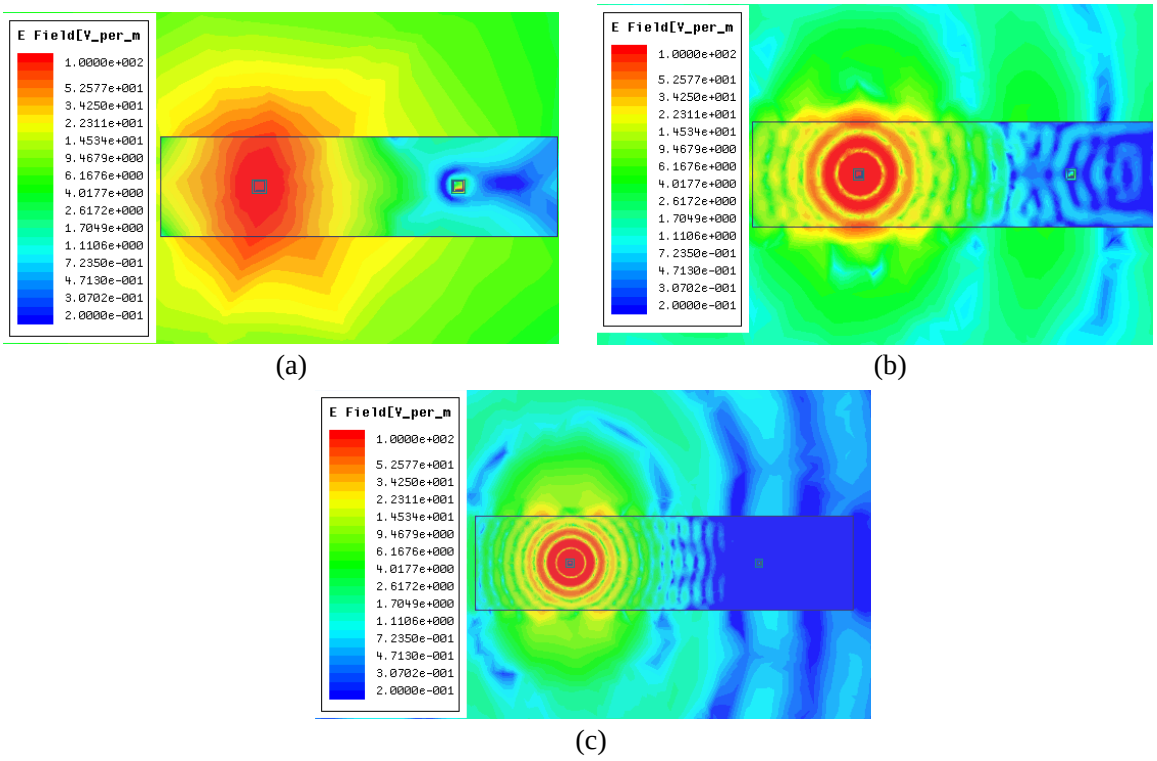

Figure 5. Magnitude of electric field inside muscle model at (a) MICS band, (b) ISM band, and (c) 3.5 GHz band.

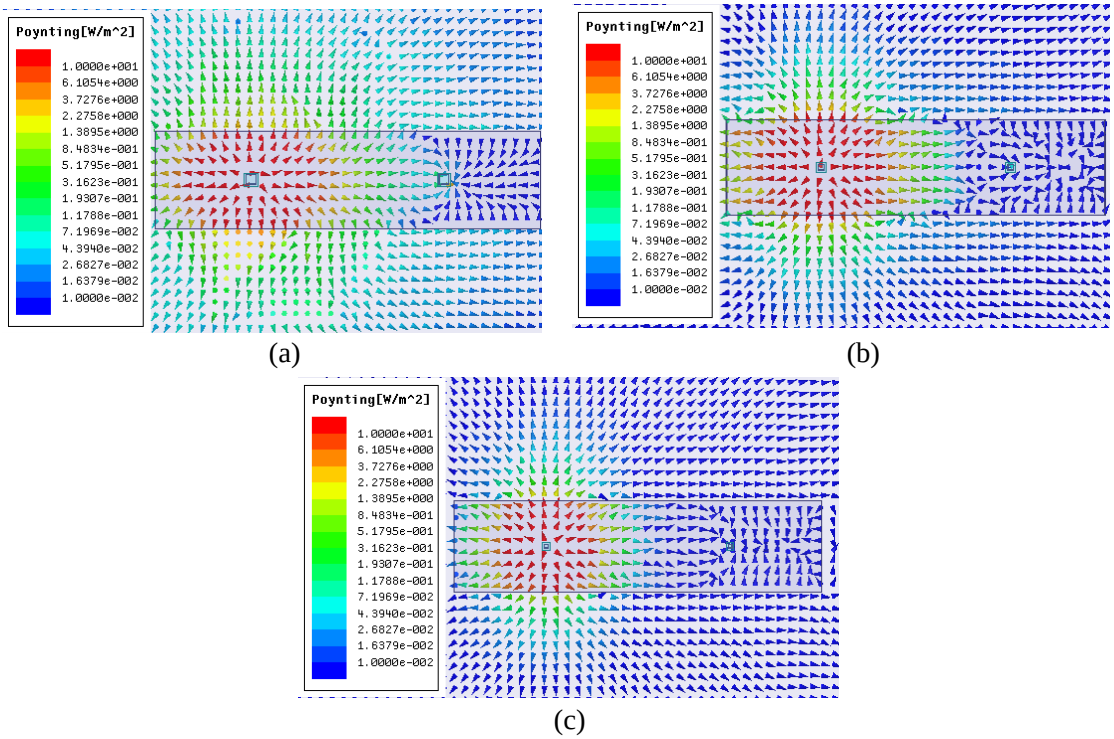

Figure 6. Real part of the Poynting vector inside muscle model at (a) MICS band, (b) ISM band, and (c) 3.5 GHz band.

near-field behavior of small antennas [12], the exponential decay is an essential component of propagation loss. Away from the transmitting antenna, an interesting phenomenon arises; our computation shows that energy reenters the body from different directions, especially at MICS band, which may be the dominant communication link at larger distances. Basically, the LOS link may not be the dominant propagation channel at a distance far away from the antenna. The energy exits the body, travels around the body and gradually enters the body from the surface (Figure 5). This effect is more prominent at the MICS frequency band. This makes the MICS band a suitable frequency band for inter and intra-body communication applications. Therefore, in the remaining parts of this paper, PL will be explained in detail inside the human body at MICS band.

5. EFFECT OF HUMAN BODY MODEL ON PL

To study the effects of human body model on PL, a one-layer human body model with different electric properties and antenna locations will be investigated at the MICS frequency band using HFSS.

5.1. Effect of Model Electric Properties

A block of dimensions $200 \times 50 \times 50\,\text{mm}^3$ with different electric properties is used to study the variations of PL due to tissue properties inside the human arm at MICS frequency band. As the first scenario, PL at different distances between transmitter and receiver is computed for the arm model with $\varepsilon_r = 53.8$ and different values of σ and the results are shown in Figure 7. These results show that the conductivity of tissues affect the PL significantly. Some approximate behavior can be concluded due to the results presented in Figure 7 as a quasilinear relationship between conductivity and the insertion loss in dB scale.

The second scenario is setup to study the effect of ε_r on PL. The same arm model is filled out with a material with $\sigma = 1.18$ and various ε_r and the PL is computed for different distances between transmitter and receiver. The simulation results presented in Figure 8 show that ε_r does not affect the PL significantly. Also, it can be seen from Figure 7 that at some particular distance between Transmitting (Tx) and Receiving (Rx) antennas, for each value of σ, the PL curve versus distance reaches a breaking point and after that the curve shows different behavior. Based on the previous discussion, the breaking point happens at the distance where the LOS link is not the dominant propagation link and the field impinging the body from the side takes the dominant effect. Therefore, the propagation mechanism changes and the curve shows different behavior.

Our simulation results agree with the theoretical results for wave propagation inside a lossy medium [18]. For plane wave propagation inside a lossy medium, PL in dB scale is linearly proportional to the attenuation coefficient α.

$$\text{PL}\,(\text{dB}) \propto \alpha \tag{1}$$

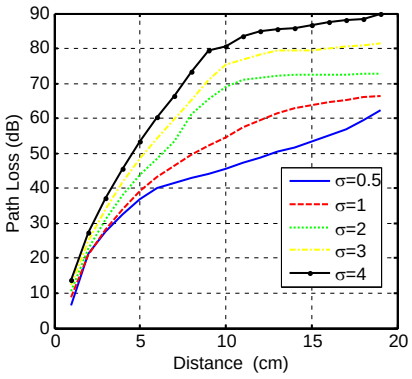

Figure 7. PL inside human body model at constant $\varepsilon_r = 53.8$ and different values of σ.

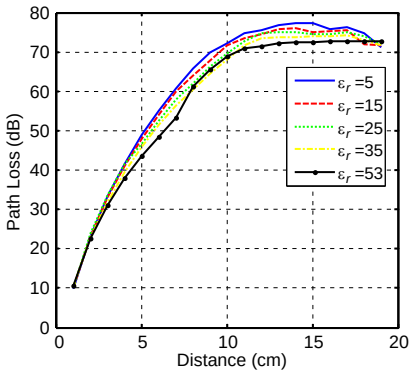

Figure 8. PL inside human body model at constant $\sigma = 1.18$ and different ε_r.

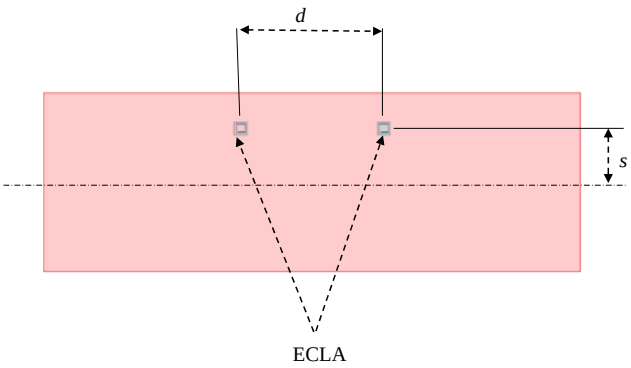

Figure 9. Two ECLAs inside one-layer muscle equivalent human body model at different ECLA locations.

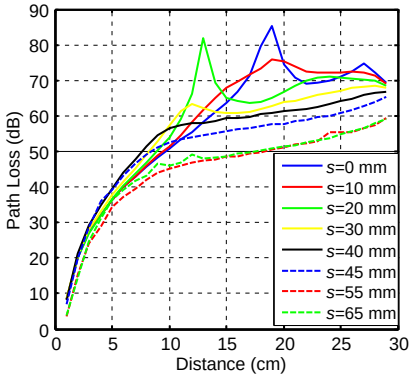

Figure 10. PL inside one-layer muscle equivalent human body model with different ECLA locations.

5.2. Effect of Antenna Position on PL

The propagation mechanism inside human body is a function of the position of the implant in the body and its distance from the surface. In this part, the effect of antenna position inside the human body model on PL will be investigated using HFSS, as shown in Figure 9. A muscle equivalent model with dimensions $300 \times 100 \times 100\,\text{mm}^3$, as a simple model for part of human leg, is used and the distance of the ECLA from the center of the model will vary from $s = 0\,\text{mm}$ (ECLAs are located at the center of the model) to $s = 65\,\text{mm}$ (ECLAs are located 15 mm above the leg model in free space). The ECLA is tuned to resonate at MICS band using the feeding head and distributed capacitor dimensions for all different scenarios. PL inside the leg model at the MICS band with different antenna heights is shown in Figure 10.

Based on these results, at $s = 55\,\text{mm}$ and $s = 65\,\text{mm}$ where the ECLAs are located in free space, PL is nearly the same and so the human body has a negligible effect on PL. At $s = 45\,\text{mm}$, where ECLAs are located 5 mm below the surface of the model, PL increases around 10 dB above that of free space. As the ECLAs' location moves deeper inside the human body, PL increases and shows some peaks due to the multipath fading of the signal. The wave exits the body, travels around the body and reenters the body from another direction, which forms a standing wave pattern inside the human body model.

6. PL INSIDE SIMPLE HUMAN BODY MODEL

To find an approximate value for PL inside the human body a simple human body model is used as shown in Figure 11. Nine ECLAs are placed inside the model at different locations. The scattering matrix (S) between all nine ECLAs is shown in (2), and the magnitude of electric field and real part of the Poynting vector are shown in Figure 12. One can see from these figures that the spherical wave radiated from the transmitting antenna decays rapidly by distance. Far from the transmitting antenna, the communication channel is through the wave which excites the body and travels around the body and reenter at each point of the body. The maximum computed loss through this model is 135 dB.

$$S\,(\text{dB}) = -\begin{bmatrix} 12 & 89 & 100 & 118 & 129 & 89 & 100 & 118 & 135 \\ 89 & 12 & 81 & 102 & 102 & 94 & 107 & 114 & 110 \\ 100 & 81 & 12 & 108 & 119 & 108 & 86 & 122 & 134 \\ 118 & 102 & 108 & 12 & 112 & 113 & 122 & 86 & 128 \\ 129 & 102 & 119 & 112 & 12 & 111 & 133 & 130 & 93 \\ 89 & 94 & 108 & 113 & 111 & 12 & 81 & 101 & 102 \\ 100 & 107 & 86 & 122 & 133 & 81 & 12 & 109 & 119 \\ 118 & 114 & 122 & 86 & 130 & 101 & 109 & 12 & 111 \\ 135 & 110 & 134 & 128 & 93 & 102 & 119 & 111 & 12 \end{bmatrix} \tag{2}$$

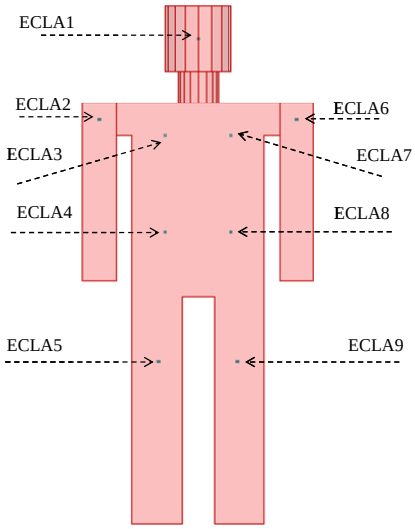

Figure 11. Locations of nine ECLAs inside one-layer muscle equivalent human body model.

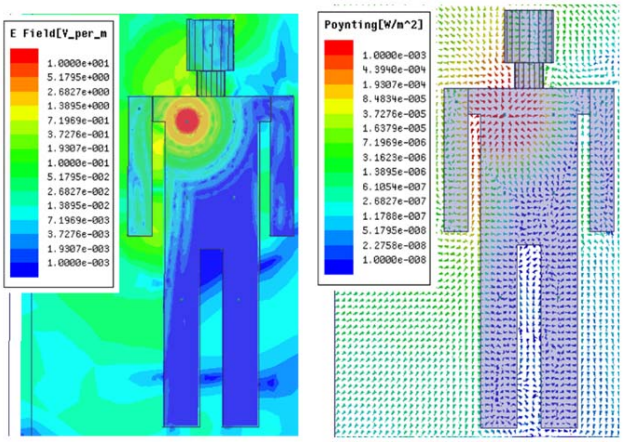

Figure 12. Magnitude of electric field and real part of Poynting vector inside one-layer muscle equivalent human body model.

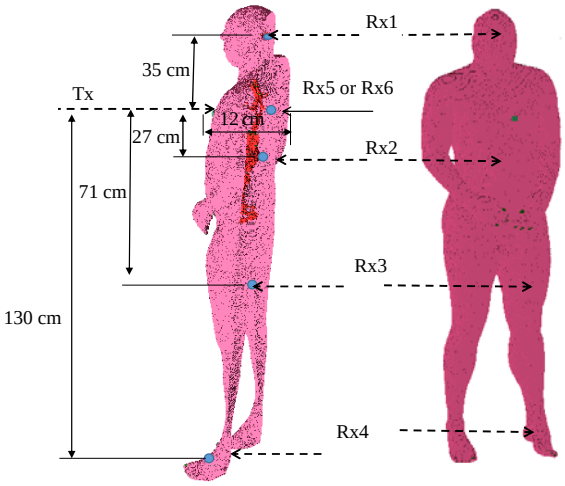

Figure 13. ECLAs with detailed human body model at different locations and cutting plane to show distances between ECLAs.

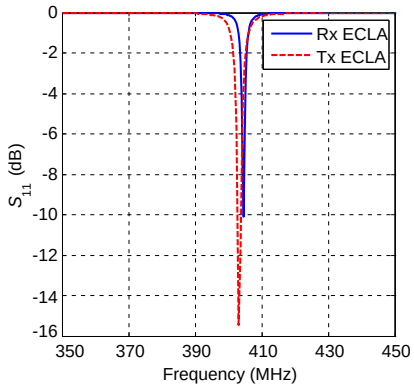

Figure 14. Scattering parameters (S_{11}) of ECLA with human body model.

Table 3. PL between ECLAs inside exact human body model.

ECLA	PL (dB)	Distance (cm)
(Tx, Rx1)	76	35
(Tx, Rx2)	81	27
(Tx, Rx3)	86.4	71
(Tx, Rx4)	89	130
(Tx, Rx5)	45	12
(Tx, Rx6)	40	12

7. PL INSIDE EXACT HUMAN BODY MODEL

The simple model used in the previous section is replaced with a more realistic model to compute the PL more accurately. Practical WBAN channel model is investigated using Remcom's XFDTD 7 (XF7) simulation software, in which a model of the human body is created, consisting of 39 human tissues. The transmitting (Tx) antenna is an ECLA with dimensions $20 \times 20 \times 5\,\text{mm}^3$ and it is located 2 mm above the skin on the chest. All the Receiving (Rx1 : Rx5) antennas are ECLAs with dimensions $5 \times 5 \times 3\,\text{mm}^3$ and are installed at different locations inside the human body as shown in Figure 13. An ECLA with dimensions $10 \times 10 \times 3\,\text{mm}^3$ (Rx6) is placed inside the human body, aligned with the transmitter, at 12 cm distance as well. Transmitting and receiving ECLAs are tuned to have a resonant frequency at the MICS band as shown in Figure 14. Table 3 shows PL between the transmitting and receiving antennas with different distances between ECLAs. From these results, maximum PL between the external transmitting and implanted receiving antennas at different locations inside the human body is about 90 dB. Also, antenna size reduction from $10 \times 10 \times 3\,\text{mm}^3$ to $5 \times 5 \times 3\,\text{mm}^3$ increases PL by 5 dB.

8. EXPERIMENTAL WORKS

Two ECLAs with dimensions $20 \times 20 \times 5\,\text{mm}^3$ and $5 \times 5 \times 3\,\text{mm}^3$ are designed and built as transmitting and receiving antennas respectively. A box with dimensions $30 \times 20 \times 10\,\text{cm}^3$ filled with ground pork is used as a one-layer model. Receiving ECLA is located at a depth of 7 cm inside the ground pork, and the

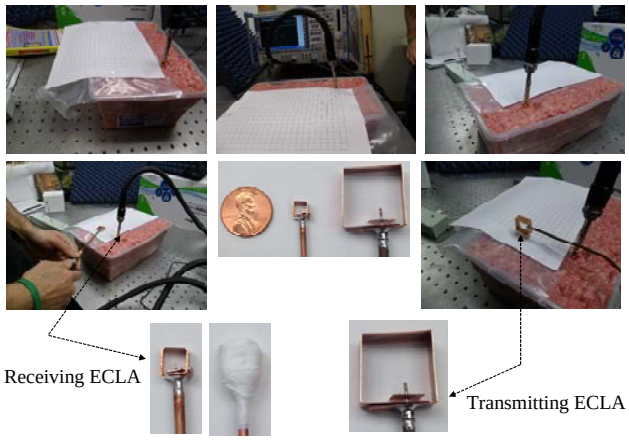

Figure 15. Scattering parameters of Tx and Rx ECLA with ground pork.

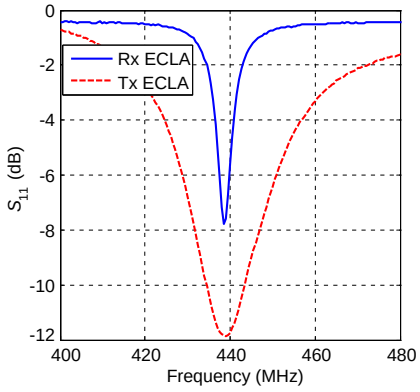

Figure 16. Scattering parameters of Tx and Rx ECLA with ground pork.

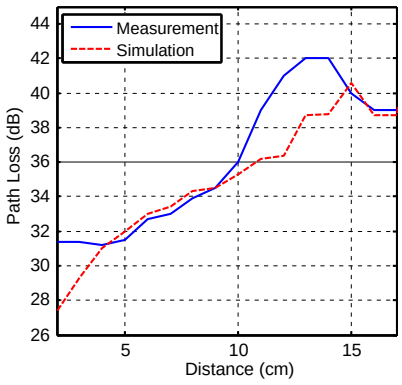

Figure 17. Experimental and simulation PL between two ECLAs using ground pork.

transmitting ECLA is located 2 mm above the surface. The horizontal distance between transmitting and receiving antenna varies from 2 to 17 cm (Figure 15). Both antennas are tuned around 440 MHz and their scattering parameters (S_{11}) are shown in Figure 16. The resonance frequency of the two ECLAs is changed due to the lumped capacitor value (29 pF in simulation and 20 pF in experimental works). PL between the two ECLAs obtained using both HFSS and experimental work is shown in Figure 17. From this figure, we see that the experimental and simulation results have a good agreement, with small differences due to measurement error. Comparing these experimental results with those in Table 3, we see that they are approximately the same. At a distance of 12 cm, simulations showed PL in the body to be 45 dB, and our measured PL in the ground pork model is 42 dB. Thus, the simulation work described in the paper is validated by experimental work.

9. CONCLUSION

Intra-body propagation channel inside the human body model was investigated using ECLAs, specifically in terms of PL which includes antenna loss, near-field loss, and path loss. In the beginning, the performance of ECLAs inside the human body models at the allowed frequency bands was investigated. It was found that as the frequency increase the allowed input power to the antenna decreases due to the higher thermal loss. The effects of certain parameters, namely operating frequency, antenna location, and human body parameters on PL were investigated. It was found that the MICS band is the most suitable band for a propagation channel inside the human body model. Based on this study, the maximum PL inside the human body is about 90 dB at MICS band for an antenna size of $20 \times 20 \times 5\,\text{mm}^3$ as the external transmitting antenna and $5 \times 5 \times 3\,\text{mm}^3$ as the implanted receiving antenna.

REFERENCES

1. Von Arx J. A. and K. Najafi, "A wireless single-chip telemetry-powered neural stimulation system," *1999 IEEE International Solid-State Circuits Conference, Digest of Technical Papers, ISSCC*, 214–215, 1999.
2. Khaleghi A. and I. Balasingham, "On the ultra wideband propagation channel characterizations of the biomedical implants," *IEEE 69th Vehicular Technology Conference, VTC Spring 2009*, 1–4, 2009.
3. Gupta, S. K. S., S. Lalwani, Y. Prakash, E. Elsharawy, and L. Schwiebert, "Towards a propagation model for wireless biomedical applications," *IEEE International Conference on Communications, ICC' 03*, Vol. 3, 1993–1997, 2003.
4. Khaleghi, A., R. Chávez-Santiago, and I. Balasingham, "Ultra-wideband statistical propagation channel model for implant sensors in the human chest," *IET Microwaves, Antennas & Propagation*, Vol. 5, 1805–1812, 2011.
5. Wang, Q., K. Masami, and J. Wang, "Channel modeling and BER performance for wearable and implant UWB body area links on chest," *IEEE International Conference on Ultra-Wideband, ICUWB 2009*, 316–320, 2009.
6. Støa, S., R. Chavez-Santiago, and I. Balasingham, "An ultra wideband communication channel model for the human abdominal region," *2010 IEEE GLOBECOM Workshops (GC Wkshps)*, 246–250, 2010.
7. Khaleghi, A., R. Chavez-Santiago, and I. Balasingham, "An improved ultra wideband channel model including the frequency-dependent attenuation for in-body communications," *2012 Annual International Conference of the IEEE Engineering in Medicine and Biology Society (EMBC)*, 1631–1634, 2012.
8. Sayrafian-Pour, K., W.-B. Yang, J. Hagedorn, J. Terrill, and K. Y. Yazdandoost, "A statistical path loss model for medical implant communication channels," *2009 IEEE 20th International Symposium on Personal, Indoor and Mobile Radio Communications*, 2995–2999, 2009.

9. Shi, J. and J. Wang, "Channel characterization and diversity feasibility for in-body to on-body communication using low-band UWB signals," *2010 3rd International Symposium on Applied Sciences in Biomedical and Communication Technologies (ISABEL)*, 1–4, 2010.
10. De Santis, V. and M. Feliziani, "Intra-body channel characterization of medical implant devices," *EMC Europe 2011 York*, 816–819, 2011.
11. Alomainy, A., Y. Hao, Y. Yuan, and Y. Liu, "Modelling and characterisation of radio propagation from wireless implants at different frequencies," *The 9th European Conference on Wireless Technology*, 119–122, 2006.
12. Manteghi, M. and A. Ibraheem, "On the study of the near-fields of electric and magnetic small antennas in lossy media," *IEEE Transactions on Antennas and Propagation*, Vol. 62, 1–6, 6491–6495, Dec. 2014.
13. Manteghi, M., "Electrically coupled loop antenna as a dual for the planar inverted-F antenna," *Microwave and Optical Technology Letters*, Vol. 55, 1409–1412, 2013.
14. Ibraheem, A. and M. Manteghi, "Performance of an implanted electrically coupled loop antenna inside human body," *Progress In Electromagnetics Research*, Vol. 145, 195–202, 2014.
15. Online: http://transition.fcc.gov/oet/rfsafety/dielectric.html.
16. "Human exposure to electromagnetic fields, high frequency (10 kHz to 300 GHz)," E. R. Committee, 1995.
17. "In the matter of guidelines for evaluating the environmental effects of radiofrequency radiation," US Federal Communications Commission, 1996.
18. Kurup, D., W. Joseph, G. Vermeeren, and L. Martens, "In-body path loss model for homogeneous human tissues," *IEEE Transactions on Electromagnetic Compatibility*, Vol. 54, 556–564, 2012.